


Properties of nonclassical correlated Stokes–anti-Stokes photon pair in decane

Filomeno S. de Aguiar Júnior ^{1,2,*} Carlos H. Monken,¹ and Ado Jorio^{1,†}

¹*Departamento de Física, ICEx, Universidade Federal de Minas Gerais, Avenida Antonio Carlos, 6627, Belo Horizonte, Minas Gerais 31270-901, Brazil*

²*Department of Chemistry, University of Victoria, Victoria, British Columbia V8W 2Y2, Canada*

 (Received 17 November 2023; revised 10 December 2023; accepted 11 December 2023; published 9 January 2024)

In this study, the correlated Stokes–anti-Stokes Raman scattering, denominated as the SaS process, is investigated in a decane sample, generalizing for a liquid the results observed in crystalline diamond. The production of SaS photon pairs is observed in both real and virtual processes by measuring nonclassical values of the second-order cross-correlation function $g_{\text{SaS}}^2(0)$. The correlated Raman spectrum is observed only for Raman shift values below approximately 2900 cm^{-1} , which is equivalent to the highest vibrational mode of the decane molecule. Furthermore, despite the fact that decane is a liquid, the polarization and spatial profile of the SaS process in decane presents the same properties as those observed in diamond.

DOI: [10.1103/PhysRevB.109.024304](https://doi.org/10.1103/PhysRevB.109.024304)

I. INTRODUCTION

The production of correlated Stokes (S) and anti-Stokes (aS) photons in the inelastic scattering of light, named the SaS Raman scattering, was predicted in 1977 by Klyshko [1], and it has been demonstrated and studied within the electronic Raman scattering in gases [2,3] and the phonon-mediated Raman scattering in diamond [4,5]. More recently, the phonon-mediated SaS Raman scattering process was identified in microelectronic devices [6], low-dimensional graphene [7] and in liquids, including water [8] and different hydrocarbons [9].

Similar to coherent anti-Stokes Raman spectroscopy (CARS), the SaS is a four-wave mixing process, which can be described by a third-order susceptibility ($P_i = \chi_{ijkl}^{(3)} E_j E_k E_l$). The difference is that CARS is an induced process that requires two lasers (the pump and the probe) to generate the aS amplified beam, while the SaS process is spontaneous, i.e., there is only one excitation laser and two photons from the laser are converted into the Stokes and anti-Stokes photon pair spontaneously.

The SaS Raman scattering as proposed by Klyshko is a resonant process, in the sense that the aS and S Raman shifts of the scattered photons with respect to the incident laser correspond respectively to plus and minus a real transition in the material, i.e., an electronic transition on the electronic Raman scattering in gases or a vibrational transition in the phonon-mediated Raman scattering in solids and liquids. As such, it has been explored experimentally and theoretically as a read-write quantum memory, as generator of an $N = 1$ phonon Fock state and as inductor of quantum correlations [4–6,8,10–12].

The SaS process has also been observed out of resonance, named virtual SaS Raman scattering, where the scattering

presents a formalism analogous to the formation of Cooper pairs in electronic superconductivity [9,13–15]. In this formalism, the SaS virtual process occurs only when the frequency of the virtual phonon is below the real phonon frequency, as it was demonstrated in diamond [16] and in water [9].

In liquid samples, the observation of Stokes–anti-Stokes correlated photon pair has been associated with a single-molecule event. However, in a recent study, Vento *et al.* [17] demonstrated that the Stokes and anti-Stokes correlations can result from a collective behavior of molecules, where a coherent vibrational mode can be shared among them.

In this work, we study the SaS process in liquid decane sample. The decane is a hydrocarbon (molecular formula $\text{C}_{10}\text{H}_{22}$). As we can see in the Fig. 1, in the Raman spectra acquired using 633 nm continuum laser (black line), the long-chain molecule $\text{C}_{10}\text{H}_{22}$ presents a complex vibrational Raman spectra, with at least 33 Raman peaks between 200 cm^{-1} and 1500 cm^{-1} and others between 2500 cm^{-1} and 3000 cm^{-1} [18,19], where the real SaS process can take a place. The maximum intensity peak of the decane Raman spectra is around 2857 cm^{-1} , associated with the C–H stretching modes. For the region, approximately from 1500 cm^{-1} to 2500 cm^{-1} , there are no Raman peaks, where we can only observe virtual SaS scattering. The light red filled area spectra in Fig. 1 was acquired using a 633 nm pulsed laser with the peaks corresponding to the convolution of the Raman peaks with the laser pulse width. In both continuum (black) and pulsed laser spectra, the anti-Stokes signal is too weak, being necessary a long accumulation time to be detected by a CCD with good spectral resolution.

We organized this paper into three more sections. In Sec. II, Methods, we talk about the experimental characteristics of the optical setup used to investigate the SaS process in this work. In Sec. III, we present the results separated into four sections, addressing different properties of the SaS process investigated: Sec. III A where we obtained the Stokes–anti-Stokes coincidences spectra; Sec. III B is about the polarization

*filomenojunior@uvic.ca

†adojorio@fisica.ufmg.br

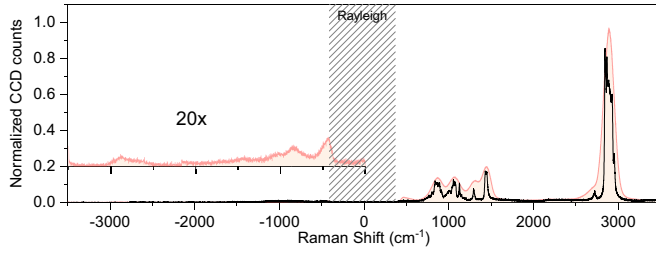


FIG. 1. Raman spectra of decane liquid sample using 633 nm helio-neon continuum laser (black) and OPO 633 nm pulsed laser (light red filled area). The hatched area matches the Rayleigh signal blocked by the notch filter. The anti-Stokes side was amplified by 20 \times to be observable.

measurement of the SaS photon pair; Sec. III C is related to the phonon lifetime measurements exploring the pump-probe experiments; Sec. III D presents an angular dependence of the photon pair scattering. In Sec. IV, we conclude this work comparing the properties of the SaS process observed in decane with the previous results in the literature for the SaS process in diamond, especially those presented in Ref. [16].

II. METHODS

As evidenced in Fig. 1, most of the Raman Stokes (spontaneous)-generated photons are uncorrelated. The anti-Stokes photons, which depend on the previous existence of a phonon in the medium, have two sources: (i) thermally generated or (ii) generated in a Stokes process (the SaS) [20]. In general, the Stokes beam is much more intense than the anti-Stokes (see Fig. 1), and to be able to extract the pure SaS correlated photon pair, where the number of Stokes and anti-Stokes photons are the same, we have to use a time-correlation measurement system.

To investigate the correlated Stokes and anti-Stokes pair generation, we used the same experimental setup from Ref. [16]. A 633 nm pulsed laser from an optical parametric oscillator (OPO) is focused in the sample by an objective lens (40 \times , 0.6 N.A.) and the transmitted signal is collected by another objective lens (100 \times , 0.9 N.A.) in a forward scattering configuration. The Rayleigh scattering is blocked by a notch filter and a beam splitter separates the Stokes (S) from the anti-Stokes (aS) signals, sending them to separated avalanche photodiode detectors (APD's). For the results in Sec. III A, while all the aS scattering is focused on the APD, the Stokes signal is filtered using a monochromator, making it possible to select the photon frequency quasicontinuously, with a spectral resolution of approximately 30 cm $^{-1}$. The APD's are connected to a time-correlated single-photon counting (TCSPC) system, the PicoHarp 300, which generates a histogram of the S and aS arrival times (see Fig. 2), for each selected Stokes frequency, giving us the number of photon pairs detected as a function of the time difference between the Stokes and anti-Stokes photon detection ($\Delta\tau$).

The peak at $\Delta\tau = 0$ ns [$I(\Delta\tau = 0)$] in the histogram corresponds to the Stokes and anti-Stokes coincidences, generated by the creation of S and aS photons in the same laser pulse due to the SaS correlated scattering process and the accidental

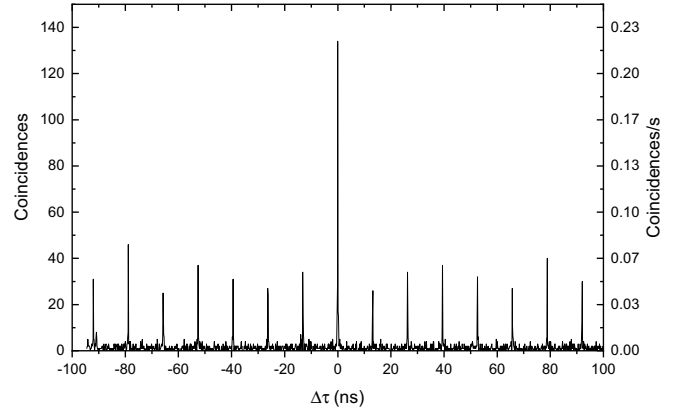


FIG. 2. Histogram for virtual SaS process at 2200 cm $^{-1}$ in decane. The histogram was acquired in 600 s exciting the sample with 42 mW of the 633 nm 200 fs, 76 MHz pulsed laser.

coincidences that can be generated by the thermal anti-Stokes Raman scattering or another source, such as fluorescence [7].

The average of the peaks at $\Delta\tau \neq 0$ ns [$\bar{I}(\Delta\tau \neq 0)$] gives a measure of the accidental coincidences, so that the SaS phenomena can be measured from:

$$I_{\text{SaS}}^{\text{Corr}} = I(\Delta\tau = 0) - \bar{I}(\Delta\tau \neq 0). \quad (1)$$

For the polarization measurements presented in the Sec. III B, we replace the monochromator by optical interference filters. We used the Stokes and anti-Stokes bandpass filters, respectively, FF01-786/22 and FF01-531/22, from Semrock, to study the SaS real process around 2900 cm $^{-1}$. To filter the virtual SaS at 2018 cm $^{-1}$ we placed in front of the Stokes and anti-Stokes APD's, respectively, the filters eo730/10 from Edmund optics and D560/40X from Chroma.

III. RESULTS

A. SaS spectrum

The average accidental coincidences [$\bar{I}(\Delta\tau \neq 0)$] increase in the real SaS process, following the same behavior of the conventional Raman scattering intensities, as we can see in Fig. 3(a), and it gives us basically the uncorrelated Raman spectrum. We also observe the increasing of coincidences at $\Delta\tau = 0$ ns [$I(\Delta\tau = 0)$ Fig. 3(b)], but not in the same rate of the accidental detection.

Looking for the counts in the histogram, we can estimate the intensity of the SaS process ($I_{\text{SaS}}^{\text{Corr}}$) by the number of SaS photon pairs detected at $\Delta\tau = 0$ ns per second, shown in the Fig. 3(b), subtracted of the accidental coincidences at zero ns per second, estimated by the average of the peaks at $\Delta\tau \neq 0$ ns [16] [Fig. 3(a)]. As a result, we obtain the SaS spectrum depicted in Fig. 3(c). We observe the maximum intensity corresponds to real SaS process, i.e., at the same Raman shift from the Raman decane peaks. While the maximum intensity of the virtual SaS scattering is close to two pairs of photons per second, the real SaS process reaches values close to 20 pairs of photons per second around 2900 cm $^{-1}$. For Raman shift above the highest frequency of the decane Raman mode, $I_{\text{SaS}}^{\text{Corr}}$ goes to zero. This result is consistent with the behavior observed in water [9] and in diamond [16,21].

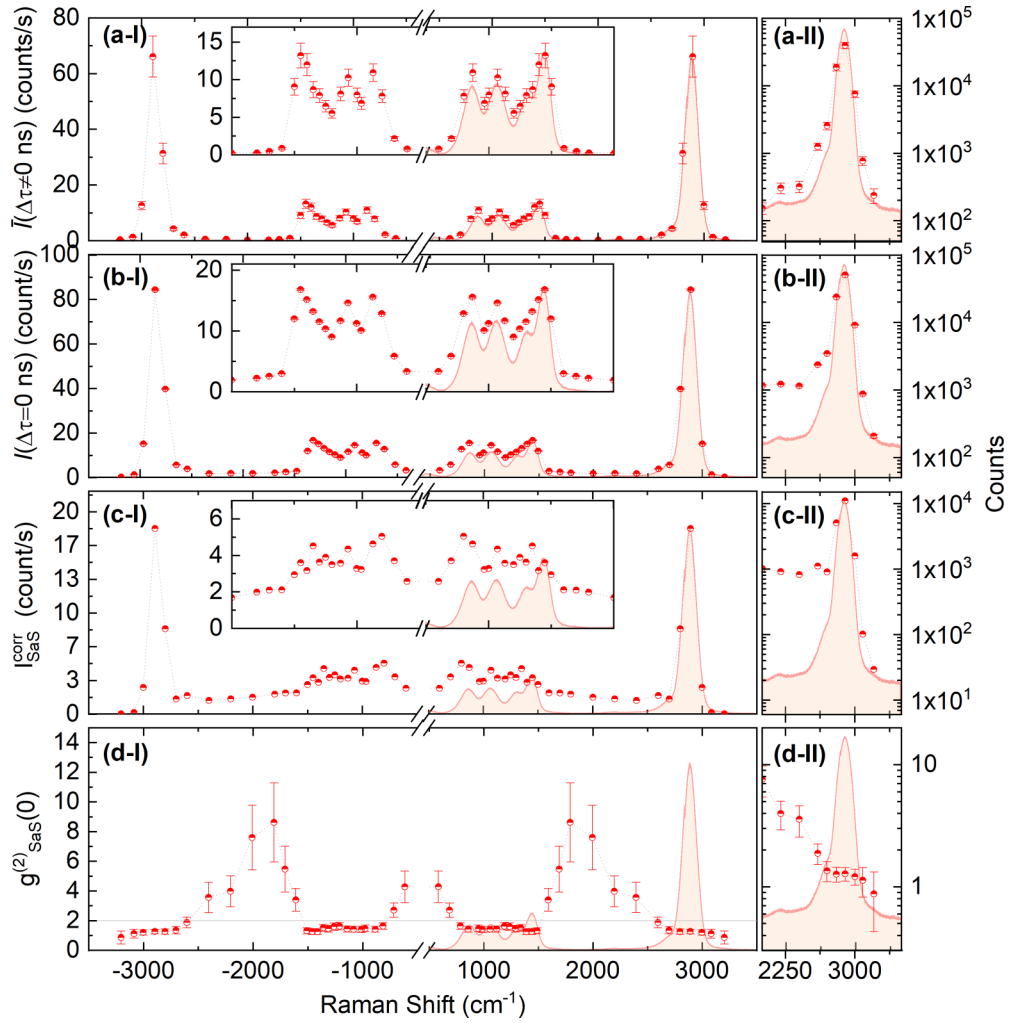


FIG. 3. (a) $\bar{I}_{\text{SaS}}(\Delta\tau \neq 0)$: average accidental coincidences per second, estimated from the average of peaks at $\Delta\tau \neq 0$ ns in the histogram. (b) $I_{\text{SaS}}(\Delta\tau = 0)$: coincidence counts per second at $\Delta\tau = 0$ ns. (c) Correlated Raman spectrum: $I_{\text{SaS}}^{\text{Corr}}$ as a function of the Raman shift, obtained by the coincidences at $\Delta\tau = 0$ ns shown in graph (b) minus the accidental coincidence exhibited in graph (a). (d) Cross-correlation function, $g_{\text{SaS}}^2(0)$, obtained from the ratio between the number of coincidences at $\Delta\tau = 0$ ns and the average of accidental at $\Delta\tau \neq 0$ ns. Each point in these graphs are obtained from a correspondent histogram acquired in 600 s, referent to Stokes filtering. The break in the spectrum corresponds to the Rayleigh signal blocked by the notch filter. The inset graphs are a zoom in the y scale in the region between -2000 and 2000 cm^{-1} . The filled light red area is a reference Raman spectrum of decane obtained with the 633 nm pulsed laser. The figures II on the right side of the graphs are a zoom from 2000 cm^{-1} to 3500 cm^{-1} with the y axis in log scale, $\times 600$ s (the total of counts, except for (d-II)), showing in the behavior, as a function of the Raman shift, of: (a-II) $\bar{I}_{\text{SaS}}(\Delta\tau \neq 0)$, (b-II) $I_{\text{SaS}}(\Delta\tau = 0)$ and evidencing the asymmetry of $I_{\text{SaS}}^{\text{Corr}}$ before and after highest frequency peak in (c-II), also observed in $g_{\text{SaS}}^2(0)$ (d-II).

We verified the production of time-correlated Stokes and anti-Stokes photon pairs by measuring the second order of cross-correlation function, $g_{\text{SaS}}^2(0) = I(\Delta\tau = 0)/\bar{I}(\Delta\tau \neq 0)$ [22], observing the violation of inequality $g_{\text{SaS}}^2(0) \leq \sqrt{g_{\text{aS,aS}}^2(0)g_{\text{S,S}}^2(0)}$. The autocorrelations of thermal Raman scattering, i.e., $g_{\text{aS,aS}}^2(0) = g_{\text{S,S}}^2(0) = 2$, limits the classical values of $g_{\text{SaS}}^2(0) \leq 2$ [5,23]. As a result, once $g_{\text{SaS}}^2(0)$ is larger than 2, the scattering of quantum correlated Stokes and anti-Stokes photon pairs is shown.

Figure 3(d) shows $g_{\text{SaS}}^2(0)$ calculated as a function of the Raman shift. We find nonclassical values of $g_{\text{SaS}}^2(0)$ for Raman shifts in the range between 1500 and 2600 cm^{-1} ,

with the maximum around 1900 cm^{-1} , out of correspondent values from active Raman modes of decane, indicating the production of correlated Stokes–anti-Stokes photon pair by the virtual SaS process. $g_{\text{SaS}}^2(0)$ reaches classical levels in resonance with the active Raman modes as a consequence of an excess of the uncorrelated photon pair produced by an uncorrelated Raman scattering, masking the SaS process. However, the values of $g_{\text{SaS}}^2(0)$ remain between 1.5 and 2, indicating that the number of coincidences at $\Delta\tau = 0$ ns is larger than the accidental coincidences, which can be reduced using a spatial filter, like an iris, or even filtering the SaS by polarization selection of the S and aS photons, like we did in Sec. III B, getting nonclassical values of $g_{\text{SaS}}^2(0)$. For Raman shift above

the highest vibration mode frequency (above $\approx 3000 \text{ cm}^{-1}$), the value of $g_{\text{SaS}}^2(0)$ goes to 1, indicating the absence of any nonclassical photon pair production process, and the detected light comes from a coherent process generated by the laser.

It is here important to comment that the results in this section are a study of frequency and time correlations in Raman scattering that reveals the presence of nonclassical inelastic light scattering related to the SaS process. Similar investigations have been performed in different systems revealing the presence of nonclassical properties of light by measuring the two-photon spectra (TPS), defined by the spectral dependence of $g^2(\omega_1, \omega_2)$ at zero time delay, with the frequency of the photons [24,25], such we present in the Fig. 3(c), where ω_1 and ω_2 are, respectively, the Stokes and anti-Stokes frequencies. As pointed out by Schmidt *et al.* [26], the TPS measurements open the possibility to explore the nonclassical process in different systems, such as plasmonic nanocavities, where the presence of plasmonic nanostructures can introduce different characteristics to the quantum correlations process in the Raman scattering.

B. Polarization of the SaS photon pair

We analyze the polarization of the S and aS photons from the SaS pair after the sample is excited by a linearly polarized laser. To perform this study, we used a set of bandpass filters (BP) to select the correspondent Stokes and the anti-Stokes signals. Then, after each band pass, a polarizer selects the polarizations of the aS and S photons. With the laser in the horizontal polarization (H) in relation to our laboratory reference system (optical table), we investigated the polarization in the virtual SaS process at around 2018 cm^{-1} , and in the real SaS process at around 2900 cm^{-1} .

Once the polarization of the excitation laser is fixed (H), we analyze the production of the SaS process in four possible polarization combinations (laser polarization; S polarization; aS polarization): (H;H;H) where the aS and S have the same polarization of the excitation, H; (H;H;V) with the S photon with polarization H and the aS photon with polarization V; (H;V;H) where the S photon has polarization V and the aS photon polarization H; and (H;V;V) indicating that the aS and S have the same polarization V, orthogonal to polarization of the laser, H.

As we can observe in Fig. 4(e), the pair of Stokes and anti-Stokes photons from a virtual SaS process has mostly the same polarization of the excitation laser, H (pink bar). The same is valid for the accidental coincidences [Fig. 4(f)]. Analyzing the true SaS coincidences, Fig. 4(g), obtained by the subtraction of the graph [Fig. 4(e)] by the graph [Fig. 4(f)], we detected around of 1.5 pair of SaS photons per second in the configurations (H;H;H), which produces $g_{\text{SaS}}^2(0) \approx 110$ [see Fig. 4(h)]. However, we also observe the SaS process in the (H;V;V) configuration, 0.06 pair per second [$g_{\text{SaS}}^2(0) \approx 15.9$], much less than in the (H;H;H) and comparable to the configuration (H;H;V), 0.013 counts/s, [$g_{\text{SaS}}^2(0) \approx 3$]. In the configuration, (H;V;H) the coincidences presents a thermal statistic, with $g_{\text{SaS}}^2(0) \approx 2$.

Studying the process at 2900 cm^{-1} , we observe similar result as the observed in the virtual process at 2018 cm^{-1} .

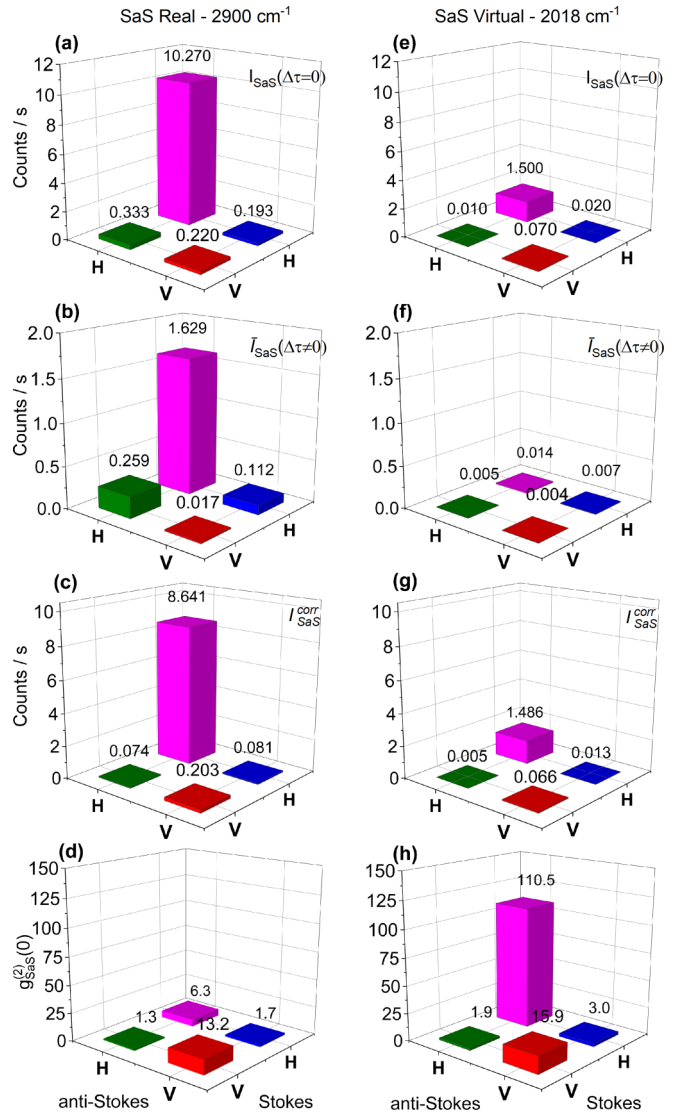


FIG. 4. Polarization studies in decane of real (left) and virtual (right) SaS scattering at 2900 cm^{-1} and 2018 cm^{-1} , respectively. (a) and (e) Absolute number of coincidences, $I_{\text{SaS}}(\Delta\tau = 0)$, defined by the absolute number of counts at $\Delta\tau = 0 \text{ ns}$ in the histograms. (b) and (f) Accidental coincidences, $\bar{I}_{\text{SaS}}(\Delta\tau \neq 0)$, defined by the average of absolute number the counts at $\Delta\tau \neq 0 \text{ ns}$ in the histograms. (c) and (g) True SaS coincidences, $I_{\text{SaS}}^{\text{corr}}$, defined by the subtraction of the accidental coincidences from the absolute coincidences. (d) and (h) Cross-correlation function, $g_{\text{SaS}}^2(0)$, estimated by the ratio between the absolute coincidence and the accidental coincidences. The experiments were performed with 20 mW of 633 nm pulsed laser from OPO.

The polarization of the SaS pairs is still determined by the incoming photons polarization once the decane Raman scattering seems to approximately depolarized, when we look for the counts detected in the Stokes APD we measure a depolarization ratio, $I_{S\perp}/I_{S\parallel} \approx 0.11$. However, as we can see comparing the real [Figs. 4(b) and 4(c)] with the virtual process [Figs. 4(f) and 4(g)], in the configuration (H;H;H), the number of SaS photon pairs increases 6 times due to the resonance with Raman modes of the decane molecule close to 2900 cm^{-1} , while the number of accidental coincidences

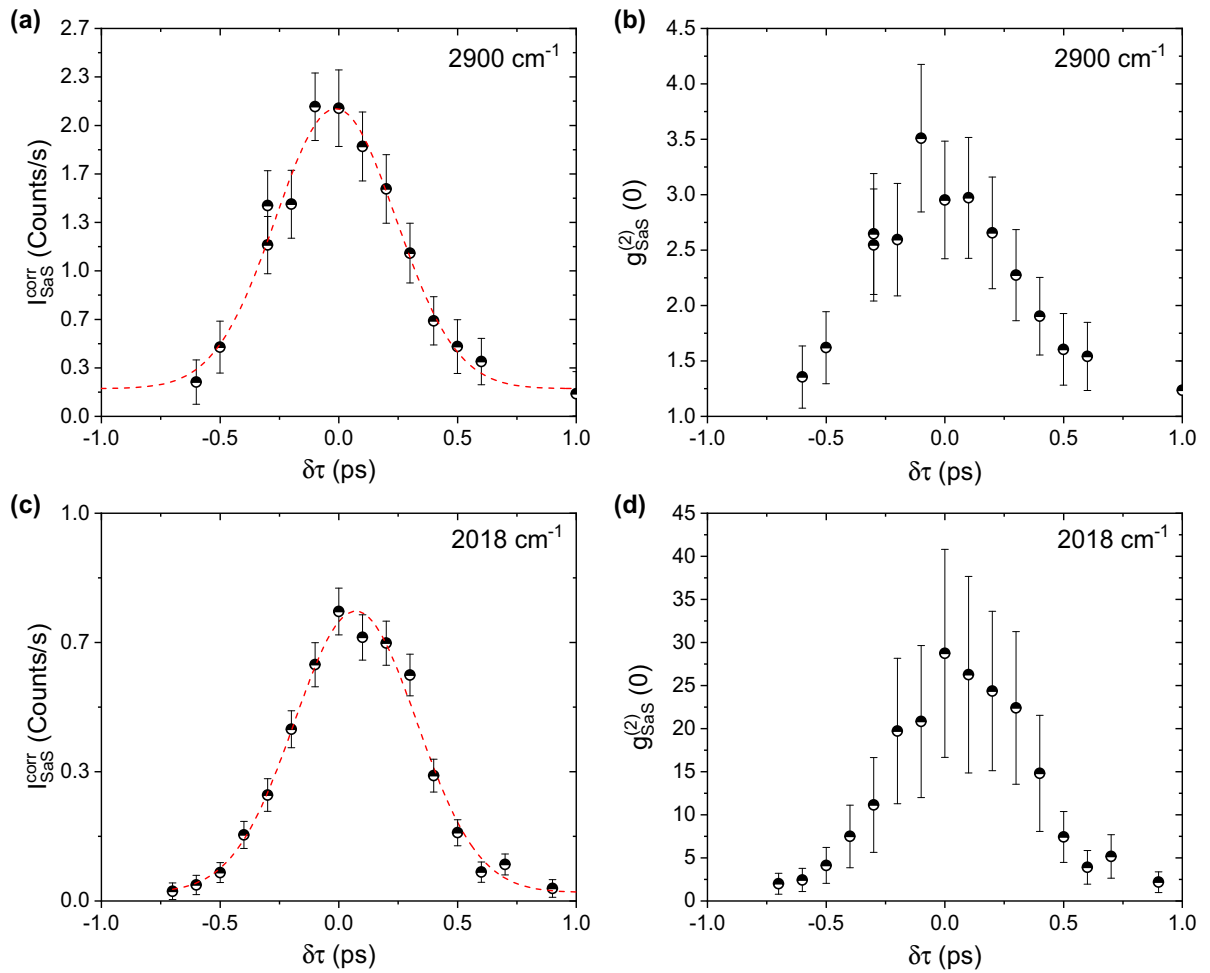


FIG. 5. Pump-probe measurements of SaS process showing in (a) the intensity, $I_{\text{SaS}}^{\text{Corr}}(\delta\tau)$, as function of the time delay $\delta\tau$ between the cross-polarized H and V laser pulses, and in (b) the cross-correlation function $g_{\text{SaS}}^2(0)(\delta\tau)$, for the real SaS process around 2900 cm^{-1} . In (c) and (d) we have, respectively, the measured values of the $I_{\text{SaS}}^{\text{Corr}}(\delta\tau)$ and $g_{\text{SaS}}^2(0)(\delta\tau)$ for the virtual process around 2018 cm^{-1} . The dashed red curves are the data fits with an Gaussian of FWHM of 0.61 ± 0.04 ps in (a) and 0.60 ± 0.03 ps in (c), resulting of the convolution of the H and V laser pulses of FWHM of, approximately 0.42 ps.

increases approximately $110\times$ times [Fig. 4(b)]. As shown in the Fig. 4(d), while in the (H;H;V) and (H;V;H) configurations $g_{\text{SaS}}^2(0) \leq 2$, mainly due to the increasing of accidental coincidences, the nonclassical Stokes–anti-Stokes scattering is observed in both (H;V;V) and (H;H;H) configurations, respectively, with $g_{\text{SaS}}^2(0) \approx 13$ and $g_{\text{SaS}}^2(0) \approx 6$.

It is important to notice that the postselection in photon polarization of the SaS pairs decrease the accidental coincidences, increasing the value of cross-correlation function. Regardless of the differences in experimental setup, comparing the Fig. 3(d) with Figs. 4(d) and 4(h), the value of $g_{\text{SaS}}^2(0)$ goes from classical [$1 \leq g_{\text{SaS}}^2(0) \leq 2$] to nonclassical value, $g_{\text{SaS}}^2(0) \approx 13$ for real process, and it increases significantly for the virtual case.

C. Pump-probe experiments

Based on previous polarization results, we conducted a pump-probe experiment exciting the sample with two cross-polarized delayed V and H laser pulses, in an effort to understand the kinetics of SaS process in the decane sample.

We used the same optical configuration from Ref. [27]. This experiment can be used to determine the vibration lifetime from the materials [27,28] and also to measure de decoherence time from the phonon [5].

By exciting the sample with two cross-polarized laser pulses separated by a temporal distance $\delta\tau$, the Stokes signal is produced by the H pulse while the anti-Stokes is mapped in the V pulses. We then studied the intensity of the SaS process as a function of the delay between the H and V pulses. Figures 5(a) and 5(b) show the results for the vibrational modes of decane molecule around 2900 cm^{-1} . We used two bandpass filters to select the Stokes and anti-Stokes signals, respectively. Due to many vibrational modes of the molecule and the large spectral width of the femtosecond laser, it is not possible select a single vibrational mode.

When we look for the intensity of the SaS process as a function of the delay time between H and V pulse, we observe the vibrational excitation created by the Stokes process do not survive more than the temporal width of the pulse. The production rate of correlated SaS photon pair is maximum when the H and V pulses are overlapped, and

decrease according the deconvolution of two pulsed lasers. The value of the cross-correlation function has the same behavior, reaching nonclassical values when the H and V pulses arrives in the sample at the same time, $\delta\tau = 0$ ps, decreasing to classical values when the overlapping between pulses decrease.

The same behavior is observed when we are looking for the virtual SaS process, around 2018 cm^{-1} for decane [see Fig. 5(c) and 5(d)]. However, the $g_{\text{SaS}}^2(0)$ always present a nonclassical value. The SaS intensity is also described by the convolution of two pulses, which is expected.

Using the 200 fs pulsed laser, we cannot resolve the temporal lifetime of the vibration excitation, once for molecules it can be less than the convolution of the two laser pulses. This is clear since both real and virtual phenomena exhibits the same temporal width (0.6 ps) in the pump-probe experiment. Also, postselecting the photon pair only by frequency and polarization, we did not observe in decane a possible collective behavior contributing for the Stokes–anti-Stokes correlation, as reported by Vento *et al.* [17] in carbon disulfide sample, when the Stokes and anti-Stokes signals are detected into a single spatial and temporal mode.

D. Spatial profile: Momentum conservation

The SaS process is observed in the forward scattering configuration, where the momentum conservation can be fulfilled. In diamond, it was demonstrated that correlated SaS photon pairs follow the laser path, i.e., without momentum scattering [16].

Analyzing the angular scattering of the virtual SaS process as in Ref. [16], where the collimated signal passes through an iris with variable radius r , we observe that the spatial profile of the SaS virtual process in decane (Fig. 6) is similar to the behavior observed in diamond. While the uncorrelated photons produced by normal Raman are scattered in all directions, the SaS is not, it is rather mostly spread within the diameter of the transmitted laser through the transparent sample due to the combined Stokes and anti-Stokes momentum conservation in the SaS process.

IV. CONCLUSION

We reproduced the same measurements performed in diamond, but looking for the SaS process generated by liquid decane that exhibits a high number of vibration modes when compared with crystals of relatively simple unit cells. As expected from the previous results [16], due to high Raman cross section, the decane shows a strong SaS photon pair production. We noticed in decane that $I_{\text{SaS}}^{\text{Corr}}$ exhibits the same spectral asymmetry as observed in Ref. [16], with lower level of SaS process at wave numbers larger than the highest vibration mode of the molecule, equivalent to the interpretation of photonic Cooper pairs proposed in Ref. [16]. The number of photon pairs produced per second for the real SaS is quite similar, despite the impact of differences in setup, alignment and laser power. While we observe around 4×10^{-4} pairs/(s mW² cm⁻¹) in decane, for diamond it was measured $\approx 6 \times 10^{-4}$ pairs/(s mW² cm⁻¹). However, the virtual process is more intense in diamond. We observed close

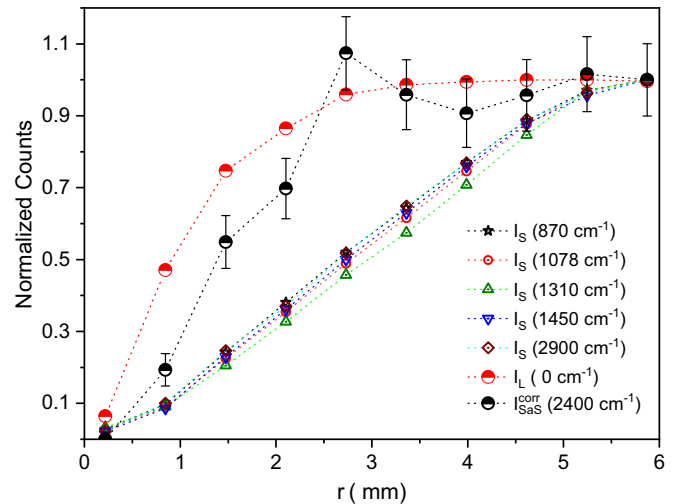


FIG. 6. Angular scattering of the virtual SaS process at 2400 cm^{-1} . Normalized intensity of the transmitted laser, normal Stokes Raman scattering, and the SaS intensity as a function of the iris radius (r), according with the legend in the figure. For the normal Raman scattering we analyse the five peaks observed in the spectrum under pulsed excitation with the intensity of Stokes obtained by the area of peaks. The anti-Stokes signal is too weak to be analyzed by the spectrometer.

to 4×10^{-5} pairs/(s mW² cm⁻¹) in decane, ten times less than detected in diamond, even when we have a comparably intense real process, showing that the difference in intensity between the virtual and real SaS process is bigger in decane than diamond. It will be interesting to investigate theoretically and experimentally the differences in efficiency, considering, for example, the difference in the index of refraction (n) between the samples (diamond has $n \approx 2.4$ and decane has $n \approx 1.4$), to improve our understanding of this phenomenon.

Regarding the polarization results, the SaS photon pair has the same polarization as the incoming laser photons, following the expected depolarization ratio of decane Raman scattering. For diamond, the polarization of the Raman signal and consequently of the SaS process depends on the symmetry of the crystal. The photon pair can have the same or an orthogonal polarization to the laser depending on the geometry of the measurements, and the orientation of the crystal relative to the excitation laser polarization. This property has been explored by Freitas *et al.* [29] observing entanglement in the virtual processes. Although molecules in liquid have random orientation in relation to the laser polarization, samples with polarized Raman scattering can be explored in the generation of entangled photons.

To summarize, the observation of correlated Raman scattering in decane presents, in general, properties similar to that observed in diamond [16], regardless the difference of physical properties of each sample, and their respective Raman scattering symmetries, showing the generality of this process. The possibility to explore the phenomena in different and also more complex systems can be the key to better understand the quantum properties of the interaction between light and matter, especially in the inelastic scattering of light.

- [1] D. N. Klyshko, Correlation between the Stokes and anti-Stokes components in inelastic scattering of light, *Sov. J. Quantum Electron. Kvantovaya Elektron. (Moscow)* **7**, 755 (1977).
- [2] M. Bashkansky, F. K. Fatemi, and I. Vurgaftman, Quantum memory in warm rubidium vapor with buffer gas, *Opt. Lett.* **37**, 142 (2012).
- [3] P. J. Bustard, J. Erskine, D. G. England, J. Nunn, P. Hockett, R. Lausten, M. Spanner, and B. J. Sussman, Nonclassical correlations between terahertz-bandwidth photons mediated by rotational quanta in hydrogen molecules, *Opt. Lett.* **40**, 922 (2015).
- [4] M. Kasperczyk, A. Jorio, E. Neu, P. Maletinsky, and L. Novotny, Stokes–anti-stokes correlations in diamond, *Opt. Lett.* **40**, 2393 (2015).
- [5] K. Lee, B. Sussman, M. Sprague, P. Michelberger, K. Reim, J. Nunn, N. Langford, P. Bustard, D. Jaksch, and I. Walmsley, Macroscopic non-classical states and terahertz quantum processing in room-temperature diamond, *Nature Photonics* **6**, 41 (2012).
- [6] R. Riedinger, S. Hong, R. A. Norte, J. A. Slater, J. Shang, A. G. Krause, V. Anant, M. Aspelmeyer, and S. Gröblacher, Non-classical correlations between single photons and phonons from a mechanical oscillator, *Nature (London)* **530**, 313 (2016).
- [7] A. Jorio, M. Kasperczyk, N. Clark, E. Neu, P. Maletinsky, A. Vijayaraghavan, and L. Novotny, Optical-phonon resonances with saddle-point excitons in twisted-Bilayer graphene, *Nano Lett.* **14**, 5687 (2014).
- [8] M. Kasperczyk, F. S. de Aguiar Júnior, C. Rabelo, A. Saraiva, M. F. Santos, L. Novotny, and A. Jorio, Temporal quantum correlations in inelastic light scattering from water, *Phys. Rev. Lett.* **117**, 243603 (2016).
- [9] A. Saraiva, F. S. de Aguiar Júnior, R. de Melo e Souza, A. P. Pena, C. H. Monken, M. F. Santos, B. Koiller, and A. Jorio, Photonic counterparts of cooper pairs, *Phys. Rev. Lett.* **119**, 193603 (2017).
- [10] K. C. Lee, M. R. Sprague, B. J. Sussman, J. Nunn, N. K. Langford, X.-M. Jin, T. Champion, P. Michelberger, K. F. Reim, D. England, D. Jaksch, and I. A. Walmsley, Entangling macroscopic diamonds at room temperature, *Science* **334**, 1253 (2011).
- [11] D. G. England, P. J. Bustard, J. Nunn, R. Lausten, and B. J. Sussman, From photons to phonons and back: A thz optical memory in diamond, *Phys. Rev. Lett.* **111**, 243601 (2013).
- [12] M. D. Anderson, S. Tarrago Velez, K. Seibold, H. Flayac, V. Savona, N. Sangouard, and C. Galland, Two-color pump-probe measurement of photonic quantum correlations mediated by a single phonon, *Phys. Rev. Lett.* **120**, 233601 (2018).
- [13] Y. Zhang, L. Zhang, and Y.-Y. Zhu, Generation of photonic cooper pairs in nanoscale optomechanical waveguides, *Phys. Rev. A* **98**, 013824 (2018).
- [14] J. Q. Shen, H. Y. Zhu, and H. L. Zhu, Photoacoustic coupling and photonic cooper pairs, *Laser & Infrared (in Chinese)* **32**, 315 (2002).
- [15] S. Timsina, T. Hammadia, S. G. Milani, F. S. de Júnior, A. Brolo, and R. de Sousa, [arXiv:2310.07139](https://arxiv.org/abs/2310.07139), (2023).
- [16] F. S. de Aguiar Júnior, A. Saraiva, M. F. Santos, B. Koiller, R. d. M. e Souza, A. P. Pena, R. A. Silva, C. H. Monken, and A. Jorio, Stokes–anti-stokes correlated photon properties akin to photonic cooper pairs, *Phys. Rev. B* **99**, 100503(R) (2019).
- [17] V. Vento, S. Tarrago Velez, A. Pogrebna, and C. Galland, Measurement-induced collective vibrational quantum coherence under spontaneous raman scattering in a liquid, *Nature Commun.* **14**, 2818 (2023).
- [18] V. Gorelik, A. Chervyakov, L. Kol'tsova, and S. Veryaskin, Raman spectra of saturated hydrocarbons and gasolines, *J. Russ. Laser Res.* **21**, 323 (2000).
- [19] E. Rosenbaum, Vibrations of long chain molecules; raman spectra of n-octane, decane, cetane and eicosane in the liquid state, *J. Chem. Phys.* **9**, 295 (1941).
- [20] C. A. Parra-Murillo, M. F. Santos, C. H. Monken, and A. Jorio, Stokes–anti-stokes correlation in the inelastic scattering of light by matter and generalization of the bose-einstein population function, *Phys. Rev. B* **93**, 125141 (2016).
- [21] L. V. Carvalho, T. A. Freitas, P. Machado Sr, R. Correa, M. F. Santos, C. H. Monken, and A. Jorio, Properties of correlated stokes-anti-stokes raman scattering from diamond, in *Ultrafast Nonlinear Imaging and Spectroscopy X*, Vol. 12228 (SPIE, Bellingham, 2022), pp. 5–8.
- [22] A. Kuzmich, W. Bowen, A. Boozer, A. Boca, C. Chou, L.-M. Duan, and H. Kimble, Generation of nonclassical photon pairs for scalable quantum communication with atomic ensembles, *Nature (London)* **423**, 731 (2003).
- [23] R. Loudon, *The quantum theory of light* (Oxford University Press, Oxford, 2000).
- [24] E. del Valle, A. Gonzalez-Tudela, F. P. Laussy, C. Tejedor, and M. J. Hartmann, Theory of frequency-filtered and time-resolved n -photon correlations, *Phys. Rev. Lett.* **109**, 183601 (2012).
- [25] G. Nienhuis, Spectral correlations in resonance fluorescence, *Phys. Rev. A* **47**, 510 (1993).
- [26] M. K. Schmidt, R. Esteban, G. Giedke, J. Aizpurua, and A. González-Tudela, Frequency-resolved photon correlations in cavity optomechanics, *Quantum Sci. Technol.* **6**, 034005 (2021).
- [27] F. S. de Aguiar Júnior, M. F. Santos, C. H. Monken, and A. Jorio, Lifetime and polarization for real and virtual correlated stokes-anti-stokes raman scattering in diamond, *Phys. Rev. Res.* **2**, 013084 (2020).
- [28] R. A. Diaz, C. H. Monken, A. Jorio, and M. F. Santos, Effective hamiltonian for stokes–anti-stokes pair generation with pump and probe polarized modes, *Phys. Rev. B* **102**, 134304 (2020).
- [29] T. A. Freitas, P. Machado, L. Valente, D. Sier, R. Corrêa, R. Saito, C. Galland, M. F. Santos, C. H. Monken, and A. Jorio, Microscopic origin of polarization-entangled Stokes–anti-Stokes photons in diamond, *Phys. Rev. A* **108**, L051501 (2023).